arXiv:2110.04085v3 [cond-mat.stat-mech] 9 May 2022

Eigenstate thermalization hypothesis and its deviations from random-matrix theory beyond the thermalization time

Jiaozi Wang,[1,*] Mats H. Lamann,[1] Jonas Richter,[2] Robin Steinigeweg,[1] Anatoly Dymarsky,[3,4,5] and Jochen Gemmer[1,†]

[1] *Department of Physics, University of Osnabrück, D-49076 Osnabrück, Germany*
[2] *Department of Physics and Astronomy, University College London, Gower Street, London WC1E 6BT, UK*
[3] *Moscow Institute of Physics and Technology, 9 Institutskiy pereulok, Dolgoprudny, Russia*
[4] *Skolkovo Institute of Science and Technology, Skolkovo Innovation Center, Moscow, Russia*
[5] *Department of Physics, University of Kentucky, Lexington, Kentucky, USA*

The Eigenstate Thermalization Hypothesis (ETH) explains emergence of the thermodynamic equilibrium in isolated quantum many-body systems by assuming a particular structure of observable's matrix elements in the energy eigenbasis. Schematically, it postulates that off-diagonal matrix elements are random numbers and the observables can be described by Random Matrix Theory (RMT). To what extent a RMT description applies, more precisely at which energy scale matrix elements of physical operators become truly uncorrelated, is however not fully understood. We study this issue by introducing a novel numerical approach to probe correlations between matrix elements for Hilbert-space dimensions beyond those accessible by exact diagonalization. Our analysis is based on the evaluation of higher moments of operator submatrices, defined within energy windows of varying width. Considering nonintegrable quantum spin chains, we observe that matrix elements remain correlated even for narrow energy windows corresponding to time scales of the order of thermalization time of the respective observables. We also demonstrate that such residual correlations between matrix elements are reflected in the dynamics of out-of-time-ordered correlation functions.

Introduction. In the overwhelming majority of cases, isolated quantum many-body systems undergoing unitary time evolution are expected to reach thermal equilibrium at long times [1–5]. During the thermalization process, local memory of the initial nonequilibrium state is lost and observables reach a constant value that agrees with an appropriate thermodynamic ensemble average, as observed in some recent experiments, see, e.g., [6–13].

Motivated by seminal works on quantum chaos and random-matrix theory (RMT), see [14–19] for reviews, including intimate connections to transport in mesoscopic systems [20, 21], the eigenstate thermalization hypothesis (ETH) explains eventual thermalization by postulating a particular structure of matrix elements of observable $\mathcal{O}$ in the eigenbasis of a generic Hamiltonian $\mathcal{H}$ [22–24],

$$\mathcal{O}_{mn} = O(\bar{E})\delta_{mn} + \Omega^{-1/2}(\bar{E}) f(\bar{E},\omega) r_{mn} \ , \qquad (1)$$

where $\omega = E_m - E_n$, $\bar{E} = (E_m + E_n)/2$, and $\mathcal{O}_{mn} = \langle m| \mathcal{O} |n\rangle$, with E_m and $|m\rangle$ denoting the eigenvalues and eigenstates of $\mathcal{H}$. Moreover, $\Omega(\bar{E})$ is the density of states, $O(\bar{E})$ and $f(\bar{E},\omega)$ are smooth functions, and the $r_{mn} = r^*_{nm}$ are usually assumed to be independent random Gaussian variables with zero mean and unit variance, see also [25–27] for early works on precursors of Eq. (1). While the general features of the ETH have been numerically confirmed for various nonintegrable models [28–38], recent works have proposed further generalizations [39–42], and scrutinized detailed aspects such as entanglement structure of highly excited eigenstates [43], or the presence of rare ETH-violating states [44].

The formulation of the ETH in Eq. (1) may essentially be regarded as an extension of the RMT applied to observables. It builds on earlier sophisticated models to describe physical systems by random matrices such as band matrices [45, 46] and embedded ensembles [18, 47–49], which take into account the locality of real systems. Numerical analyses have yielded a convincing agreement with the predictions of Eq. (1), for instance regarding the Gaussianity of the r_{mn} [35, 50], the distribution of transition strengths $|\mathcal{O}_{mn}|^2$ [51–53], and the ratio of variances of diagonal and off-diagonal matrix elements [3, 33, 34, 54]. Moreover, statistical properties of matrix elements have been analyzed semiclassically in few-body systems with classically chaotic counterpart [55–57].

Physical Hamiltonians and observables clearly differ from genuinely random operators [18] (for instance, matrix elements $\langle m| \sigma_z |n\rangle$ of a Pauli operator must be correlated to yield the eigenvalues ± 1). In this context, the question whether and to what extent the r_{mn} in Eq. (1) can indeed be considered as *uncorrelated* random numbers has attracted increased attention recently [37, 58, 59]. In particular, it has been argued that correlations between matrix elements are necessary to explain the growth of out-of-time ordered correlation function (OTOC) [60–62], which is a central quantity to characterize scrambling in quantum systems [63]. Using full eigenvalue spectrum of operator submatrices as a sensitive indicator, correlations between matrix elements have been shown to persist to small energy scales, but appear to vanish at even lower ω [37]. The lack of correlations between r_{mn} at low ω is consistent with expected universality of the observable's dynamics at late times [64–67].

An important and less clear aspect is to connect the onset of RMT behavior, particularly the statistical inde-

pendence of matrix elements, with the time scale of thermalization. Given a (one-dimensional) quantum many-body system of size L, the thermalization time $\tau_{\rm th}$ of an observable $\mathcal{O}$ is expected to scale as $\tau_{\rm th} \propto L^{\nu}$, where $\nu \geq 0$ depends on $\mathcal{O}$ and details of the system, e.g., presence of conservation laws [68], or disorder [69]. Somewhat unexpectedly, it was analytically shown in [58] that in one dimensional systems, macroscopic thermalization dynamics prevents matrix elements of $\mathcal{O}$ from becoming truly uncorrelated above a smaller energy scale $\Delta E_{\rm RMT} \propto 1/(\tau_{\rm th} L)$, and the system's dynamics is fully described by RMT only at much later times, $T_{\rm RMT} \propto 1/\Delta E_{\rm RMT} \propto \tau_{\rm th} L$. This has consequences for instance for the dynamics of certain initial states with a macroscopic spatial inhomogeneity of a conserved quantity, e.g., energy, which will display nontrivial dynamics even for $t > \tau_{\rm th}$ and saturate into exponentially small fluctuations $\propto e^{-L}$ only at parametrically longer t [58].

We note that the time $T_{\rm RMT}$ explored here and in [58], which marks the absence of correlations between matrix elements, is different from the so-called "Thouless time" [70], see [71] for details, which has also been associated to the applicability of RMT to the energy spectrum, signaled by a ramp in the spectral form factor [67, 73–76].

From a numerical point of view, a major complication to study matrix elements is given by the restriction of full exact diagonalization (ED) to small system sizes, such that the analysis of low-frequency or, correspondingly, long-time regimes is plagued by severe finite-size effects. In this Letter, we introduce a novel numerical approach based on quantum typicality (see [77, 78] and references therein). We show that moments of operator submatrices, defined within energy windows of varying width, can be evaluated for system sizes beyond the range of ED, and provide a sensitive probe to study the presence of correlations between matrix elements. This allows us to shed new light on residual deviations of physical operators from genuine RMT ensembles, including the Gaussian Orthogonal Ensemble (GOE), which is expected to emerge for the models and operators with real and symmetric matrix representation considered here. For non-integrable quantum spin chains, our analysis shows that matrix elements remain correlated even in narrow energy windows corresponding to time scales around the thermalization time of the respective observable. For shorter times, the residual correlations between matrix elements are manifest in the nontrivial dynamics of suitably defined OTOCs within such energy windows.

Setup. We consider submatrices $\mathcal{O}^T$ defined within energy windows of width $2\pi/T$ [37, 54, 58],

$$\mathcal{O}^T_{mn} = \langle m|P_T \mathcal{O} P_T|n\rangle = \begin{cases} \mathcal{O}_{mn} \ , & |E_{m,n} - E_0| \leq \frac{\pi}{T} \\ 0 \ , & \text{otherwise} \end{cases} , \tag{2}$$

where $P_T = \sum_{|E_m - E_0| \leq \frac{\pi}{T}} |m\rangle\langle m|$ is a projection on eigenstates of $\mathcal{H}$ centered around E_0. Parameter T controlling the size of the submatrix determines characteristic time scale (matrix elements at low ω contribute to dynamics at long times). We will compare the energy scale $1/T$, where the $\mathcal{O}^T_{mn}$ become uncorrelated, with the scale $1/\tau_{\rm th}$ set by thermalization time of $\mathcal{O}$. Examples of $\mathcal{H}$, $\mathcal{O}$, and a definition of $\tau_{\rm th}$ are given below.

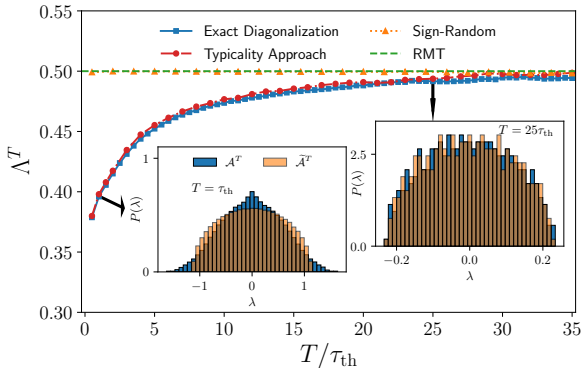


FIG. 1. Λ^T versus $T/\tau_{\rm th}$ for $\mathcal{A}$ with $q = L/2$ and $L = 16$. Results obtained by the typicality approach, averaged over 500 states, agree convincingly with ED data. As a comparison, Λ^T obtained from a sign-randomized operator [Eq. (7)] yields the GOE value $\Lambda^T = 1/2$. Insets show eigenvalue distributions $P(\lambda)$ of $\mathcal{A}^T$ and $\widetilde{\mathcal{A}}^T$ for different energy windows.

We study the presence of correlations between matrix elements by introducing the ratio Λ^T of moments of $\mathcal{O}^T_c$,

$$\Lambda^T = \mathcal{M}_2^2/\mathcal{M}_4 \ , \quad \mathcal{M}_k = {\rm Tr}[(\mathcal{O}^T_c)^k]/d \ , \tag{3}$$

where $d = {\rm Tr}[P_T] = \sum_{|E_m - E_0| \leq \frac{\pi}{T}} 1$ and $\mathcal{O}^T_c = \mathcal{O}^T - {\rm Tr}(\mathcal{O}^T)/d$. If $\mathcal{O}^T$ were to be described by an ideal GOE, its eigenvalues would follow famous Wigner semicircle distribution, implying $\Lambda^T_{\rm GOE} = 1/2$. Crucially, as we show in [79], $\Lambda^T \simeq 1/2$ can be derived also for weaker conditions on $\mathcal{O}^T$ as long as the $\mathcal{O}^T_{mn}$ are statistically independent. In particular, as discussed in [79] and demonstrated below, $\Lambda^T \to 1/2$ can serve as a sensitive indicator to locate the energy scale where $\mathcal{O}^T_{mn}$ become uncorrelated and deviations from a strict GOE disappear.

Numerical approach. To construct $\mathcal{O}^T$ explicitly without using ED, it is crucial to rewrite P_T as $P_T = \frac{1}{T}\int_{-\infty}^{+\infty} {\rm sinc}(t/T)\exp[-i(\mathcal{H} - E_0)t]dt$ [58], where ${\rm sinc}(t) = \sin(\pi t)/\pi t$. In particular, by expanding the time evolution operator in terms of Chebyshev polynomials [81–83] and evaluating the integral analytically, one finds [79], $P_T = \sum_{k=0}^{\infty} C_k T_k(\frac{\mathcal{H}-b}{a})$, where $T_k(x)$ are Chebyshev polynomials of the first kind, C_k are suitable coefficients [79], and $a = (E_{\rm max} - E_{\rm min})/2$, $b = (E_{\rm max} + E_{\rm min})/2$, where $E_{\rm max}$ ($E_{\rm min}$) is the largest (smallest) eigenvalue of $\mathcal{H}$. Exploiting quantum typicality [77, 78] (see also [79]) one can then calculate the second and the fourth central moments of $\mathcal{O}^T$ as

$$\mathcal{M}_2 \approx \frac{\langle \psi_{POP}|\psi_{POP}\rangle}{\langle \psi_P|\psi_P\rangle} \ , \ \mathcal{M}_4 \approx \frac{\langle \psi_{(POP)^2}|\psi_{(POP)^2}\rangle}{\langle \psi_P|\psi_P\rangle} \ , \tag{4}$$

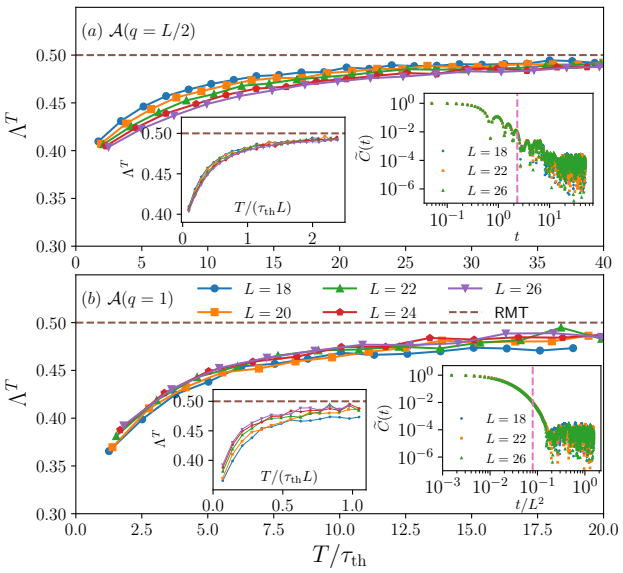


FIG. 2. Λ^T versus $T/\tau_{\rm th}$ for the density-wave operator $\mathcal{A}$ with (a) $q = L/2$ and (b) $q = 1$. Data are obtained using typicality approach up to $L = 26$, averaged over $500 \cdot 2^{16-L}$ random states [96]. The dashed line indicates the GOE value $\Lambda^T_{\rm GOE} = 0.5$. Insets show Λ^T versus $T/(\tau_{\rm th}L)$ and the rescaled correlation function $\widetilde{C}(t)$. The dashed vertical line signals $\tau_{\rm th}$ according to our definition in the text. The data collapse of $\widetilde{C}(t)$ and $\widetilde{C}(t/L^2)$ indicates L-independence of $\tau_{\rm th}$ for $q = L/2$ and diffusive behavior $\tau_{\rm th} \propto L^2$ for $q = 1$.

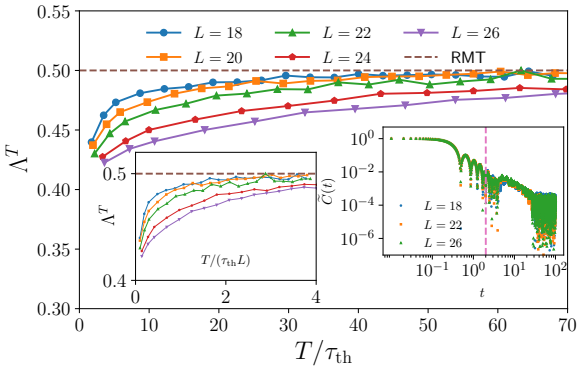


FIG. 3. Analogous data as in Fig. 2, but now for $\mathcal{B}$.

where $|\psi_P\rangle = P_T|\psi\rangle$, $|\psi_{POP}\rangle = P_T\mathcal{O}_c^T P_T|\psi\rangle$, $|\psi_{(POP)^2}\rangle = (P_T\mathcal{O}_c^T P_T)^2|\psi\rangle$, and $\mathcal{O}_c^T = \mathcal{O}^T - \langle\psi_P|\mathcal{O}^T|\psi_P\rangle/\langle\psi_P|\psi_P\rangle$. Here, $|\psi\rangle$ is a pure state drawn at random from the unitarily invariant Haar measure [84], i.e., in practice $|\psi\rangle$ is constructed in the computational basis with Gaussian distributed coefficients. The approximation of $\mathcal{M}_k$ in Eq. (4) becomes very accurate for energy windows with sufficiently many eigenstates. For smaller windows with fewer eigenstates, the accuracy can be improved by averaging over multiple realizations of $|\psi\rangle$. The most demanding step of our approach is to restrict the random state to a narrow energy window, $P_T|\psi\rangle = \sum_{k=0}^{M} C_k T_k(\frac{\mathcal{H}-b}{a})|\psi\rangle$, where P_T is approximated by a sum up to $k = M$, which has to be chosen large enough to yield accurate results [85]. Combined with efficient sparse-matrix techniques, $\mathcal{M}_k$ and Λ^T can then be obtained for Hilbert-space dimensions far beyond the range of the ED. Note that other approaches exist to construct states in a specified energy window [86–89].

Numerical analysis. We consider one-dimensional mixed-field Ising model, $\mathcal{H} = \sum_{\ell=1}^{L} \mathcal{H}^\ell$,

$$\mathcal{H}^\ell = J\sigma_z^\ell\sigma_z^{\ell+1} + \frac{h_x}{2}(\sigma_x^\ell + \sigma_x^{\ell+1}) + \frac{h_z}{2}(\sigma_z^\ell + \sigma_z^{\ell+1}) \ , \quad (5)$$

where $\sigma_{x,z}^\ell$ are Pauli operators at lattice site ℓ, L is the length of the chain with periodic boundaries, and $J = h_x = 1.0$ and $h_z = 0.5$ in the following. Moreover, we add two defect terms $h_2\sigma_z^2$ and $h_5\sigma_z^5$ with $h_2 = 0.1665$ and $h_5 = -0.2415$ to lift translational and reflection symmetries, such that our simulations are performed in the full Hilbert space of dimension 2^L. We note that $\mathcal{H}$ is nonintegrable, fulfills the ETH for these parameters [79], and exhibits diffusive energy transport [90]. We consider energy windows around $E_0 = 0$, corresponding to infinite temperature. We study Λ^T for two kinds of operators,

$$\mathcal{A} = \frac{1}{\sqrt{L}}\sum_{\ell=1}^{L}\cos\left(\frac{2\pi}{L}q\ell\right)\mathcal{H}^\ell, \quad \mathcal{B} = \frac{1}{\sqrt{L}}\sum_{\ell=1}^{L}\sigma_x^\ell \ , \quad (6)$$

where $\mathcal{B}$ exhibits no transport behavior and decays quickly. In contrast, dynamics of the density-wave operator $\mathcal{A}$ depends on q, with a quick L-independent decay for $q = L/2$ and a slow hydrodynamic (diffusive) relaxation in the limit of small q [68]. For our numerical analysis, operators with short, L-independent, $\tau_{\rm th}$ are beneficial as this allows us to reach regimes $T/\tau_{\rm th} \gg 1$, which in contrast becomes very costly if $\tau_{\rm th} \propto L^2$ scales diffusively.

A first glance of how Λ^T behaves upon varying the width of the energy window is given in Fig. 1, where we consider $\mathcal{A}$ for a small system with $L = 16$ amenable to ED. ED values of Λ^T show convincing agreement with those obtained using typicality approach for a wide range of T. Analyzing Λ^T behavior, we see that it deviates from the GOE value for small T (i.e., large energy windows), but approaches it for larger T. As shown in the insets of Fig. 1, the full eigenvalue distribution $P(\lambda)$ of $\mathcal{A}^T$ is approximately Gaussian for small T ($\Lambda^T = 1/3$ for strictly Gaussian distributions), while it takes an approximately semicircle shape for larger T, indicating a transition to GOE behavior [37]. Importantly, while Λ^T displays that strict GOE behavior only occurs at large T, other common random-matrix indicators, such as the mean ratio of adjacent level spacings $\langle r\rangle$ [91], turn out to be insensitive to the residual correlations between the $\mathcal{O}_{mn}^T$ at small T, see [79]. In this context, it is also helpful to evaluate Λ^T

for a sign-randomized version of $\mathcal{O}^T$ [37, 92, 93],

$$\widetilde{\mathcal{O}}^T_{mn} = \begin{cases} \mathcal{O}^T_{mn} \ , & 50\% \text{ probability} \\ (-1)\mathcal{O}^T_{mn} \ , & 50\% \text{ probability} \end{cases} , \tag{7}$$

where potential correlations between the $\mathcal{O}^T_{mn}$ are thus manually destroyed. As shown in Fig. 1, $\widetilde{\mathcal{A}}^T$ indeed yields $\Lambda^T \approx 0.5$ with semicircular $P(\lambda)$ for all T, which further confirms that $\Lambda^T \to 0.5$ is a good indicator for the absence of correlations between matrix elements.

We now turn to the dependence of Λ^T on T for larger systems up to $L = 26$, using our novel typicality approach. First, we consider operator $\mathcal{O} = \mathcal{A}$ with $q = L/2$, for which the infinite-temperature autocorrelation function $C(t)$ (also obtained by typicality [77–79, 94]) exhibits a short L-independent τ_{th} [Fig. 2 (a)], where

$$C(t) = \text{Tr}[\mathcal{O}(t)\mathcal{O}]/2^L \ . \tag{8}$$

We here define τ_{th} as the time when $\widetilde{C}(t) = [C(t) - C(t \to \infty)]/[C(0) - C(t \to \infty)]$ has decayed to $\widetilde{C}(t) < 0.01$ and stays below this threshold afterwards [95]. Note that by Fourier transforming $C(t)$, $2\pi/\tau_{\text{th}}$ sets the "Thouless energy" below which $f(\bar{E}, \omega)$ in Eq. (1) becomes approximately constant [71, 72]. Inspecting Λ^T at the energy scale which corresponds to thermalization, $T \approx \tau_{\text{th}}$, we find Λ^T is far from the GOE value but tends to approach it at larger values of T. The same behavior of Λ^T is also demonstrated by the second operator $\mathcal{O} = \mathcal{B}$, see Fig. 3. Specifically, $\mathcal{B}$ also has L-independent thermalization time τ_{th} and, especially for large L, Λ^T is still far from the GOE value even at long times $T \sim 20\tau_{\text{th}}$.

Next, we consider density-wave operator $\mathcal{A}$ with the longest wavelength, $q = 1$. This is a diffusive operator and $C(t)$ decays exponentially with $\tau_{\text{th}} \propto L^2$, as confirmed by the collapse of $\widetilde{C}(t/L^2)$ for different L [inset of Fig. 2 (b)]. Similar to the previous case, we find that Λ^T is far from the GOE prediction at $T \approx \tau_{\text{th}}$, while it tends to approach it for larger T. Thus, in all cases shown in Figs. 2 and 3, we conclude that matrix elements of $\mathcal{O}^T$ remain correlated around the energy scale defined by inverse thermalization time $1/\tau_{\text{th}}$, consistent with [58]. A *strict* description of $\mathcal{O}^T$ by a random matrix drawn from a GOE may therefore apply only at much longer times $T_{\text{RMT}} \gg \tau_{\text{th}}$. This is the main result of this Letter.

It would be a natural step to quantify $T_{\text{RMT}}/\tau_{\text{th}}$ for different operators, and in particular its dependence on the system size L. In practice this requires extending numerical analysis to much larger T for which $\Lambda^T \approx 0.5$, which is a challenging task. Here, we particularly focus on the case of $\mathcal{A}$ with $q = L/2$. Plotting Λ^T versus $T/(\tau_{\text{th}}L)$, see inset in Fig. 2 (a), we observe a good data collapse extending over the entire range of T shown here. This tentatively suggest $T_{\text{RMT}} \propto \tau_{\text{th}}L$ for this particular operator, which is also consistent with [97]. Furthermore, in [79], we provide additional results for a nonintegrable XXZ chain with next-nearest neighbor interactions and a local operator exhibiting diffusive transport. Also in this case, the data is consistent with $T_{\text{RMT}} \propto \tau_{\text{th}}L$. Generally, however, the universality of this scaling remains unclear since such a collapse of Λ^T is absent in other cases [cf. Figs. 2 (b) and 3]. Nevertheless, at least for $\mathcal{B}$ in Fig. 3, it appears that while $\tau_{\text{th}} \approx$ const., T_{RMT} increases with L, which supports our main result that asymptotically $T_{\text{RMT}} \gg \tau_{\text{th}}$. While a potential confirmation of $T_{\text{RMT}} \propto \tau_{\text{th}}L$ would require a collapse in the immediate region of $T \approx T_{\text{RMT}}$, this is currently beyond our numerical capabilities and we here leave to future work to develop other indicators of T_{RMT} complementary to Λ^T.

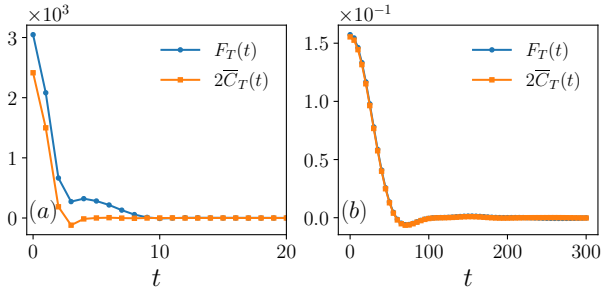


FIG. 4. $F_T(t)$ [Eq. (9)] and $2\overline{C}_T(t)$ [Eq. (10)] for $\mathcal{A}$ with $q = L/2$ and $L = 16$, for (a) $T = \tau_{\text{th}}$ and (b) $T = 25\tau_{\text{th}}$.

Dynamics of OTOCs. Correlations between $\mathcal{O}^T_{mn}$ also manifest themselves in dynamical properties [59]. In particular, we consider out-of-time-ordered correlation function, defined within the energy window $|E_m - E_0| \leq \frac{\pi}{T}$,

$$F_T(t) = \text{Tr}[\mathcal{O}^T_c(t)\mathcal{O}^T_c\mathcal{O}^T_c(t)\mathcal{O}^T_c] \ . \tag{9}$$

Assuming that off-diagonal matrix elements of $\mathcal{O}^T_c$ are uncorrelated and that diagonal elements satisfy ETH [79], $F_T(t)$ should reduce to $F_T(t) \simeq 2\overline{C}_T(t)$, where $\overline{C}_T(t)$ is the eigenstate-averaged two-point function,

$$\overline{C}_T(t) \equiv \sum_{m=1}^{d} \Re \ \langle m|\mathcal{O}^T_c(t)\mathcal{O}^T_c|m\rangle^2 \ . \tag{10}$$

In Fig. 4, $F_T(t)$ and $\overline{C}_T(t)$ are shown for the density-wave operator $\mathcal{A}$ with $q = L/2$. We consider $L = 16$ and two different energy windows, $T = \tau_{\text{th}}$ [Fig. 4 (a)] and $T = 25\tau_{\text{th}}$ [Fig. 4 (b)]. In the former case, we find $F_T(t) \neq 2\overline{C}_T(t)$, which is consistent with our earlier observation that $\Lambda^T \neq 0.5$ at $T = \tau_{\text{th}}$ [Fig. 2 (a)] and supports our conclusion that higher-order correlations exist between the $\mathcal{O}^T_{mn}$. In contrast, in the latter case, $F_T(t) \approx 2\overline{C}_T(t)$, consistent with $\Lambda^T \to 0.5$ and signaling that correlations between the $\mathcal{O}^T_{mn}$ vanish and strict GOE behavior emerges for such narrow energy windows.

Conclusion & Outlook. We have studied presence of correlations between matrix elements of observables written in the energy eigenbasis of chaotic quantum many-body systems. We introduced a novel numerical method

to evaluate higher moments of operator submatrices for system sizes beyond those accessible by ED. As a main result, we have shown that even for narrow energy windows, corresponding to time scales of the order of thermalization time for the given observable, matrix elements remain correlated. Consistent with the results of [37, 58], our findings suggest that even though usual indicators of the ETH might be completely fulfilled [79], ETH has to be refined to properly describe all dynamical aspects of thermalization. Specifically, in addition to the usual thermalization or Thouless time controlling RMT behavior of energy levels, there exists another relevant time $T_{\mathrm{RMT}} \gg \tau_{\mathrm{th}}$, which marks the end of macroscopic thermalization dynamics (see also [58]) and the scale where $\mathcal{O}^T_{mn}$ become uncorrelated. We demonstrated this fact by studying suitably defined OTOCs, which visualized the presence of correlations between $\mathcal{O}^T_{mn}$ well beyond the thermalization time of the two-point function.

A natural next step is to systematically study L dependence of $T_{\mathrm{RMT}}/\tau_{\mathrm{th}}$ for various operators and to clarify the role of conservation laws giving rise to hydrodynamic behavior at late times. While we expect that our findings can be generalized to other systems, it would be interesting to study T_{RMT} in a wider class of models, including time-dependent Floquet models without energy conservation, as well as disordered systems which may exhibit subdiffusive transport or localization depending on the disorder strength [98]. Finally, another direction is to consider few-body systems with classically chaotic counterpart and to explore T_{RMT} and its deviations from the Thouless time from a semiclassical point of view.

Acknowledgements. This work has been funded by the Deutsche Forschungsgemeinschaft (DFG), Grants No. 397107022 (GE 1657/3-2), No. 397067869 (STE 2243/3-2), and No. 355031190, within the DFG Research Unit FOR 2692. J. R. has been funded by the European Research Council (ERC) under the European Union's Horizon 2020 research and innovation programme (Grant agreement No. 853368). A. D. acknowledges support of the Russian Science Foundation (Project No. 17-12-01587).

* jiaozi.wang@uos.de
† jgemmer@uos.de

[1] A. Polkovnikov, K. Sengupta, A. Silva, and M. Vengalattore, Rev. Mod. Phys. **83**, 863 (2011).
[2] C. Gogolin and J. Eisert, Rep. Prog. Phys. **79**, 056001 (2016).
[3] L. D'Alessio, Y. Kafri, A. Polkovnikov, and M. Rigol, Adv. Phys. **65**, 239 (2016).
[4] F. Borgonovi, F. M. Izrailev, L. F. Santos, and V. G. Zelevinsky, Phys. Rep. **626**, 1 (2016).
[5] T. Mori, T. N. Ikeda, E. Kaminshi, and M. Ueda, J. Phys. B: At. Mol. Opt. Phys. **51**, 112001 (2018).
[6] S. Trotzky, Y.-A. Chen, A. Flesch, I. P. McCulloch, U. Schollwöck, J. Eisert, and I. Bloch, Nat. Phys. **8**, 325 (2012).
[7] A. M. Kaufmann, M. E. Tai, A. Lukin, M. Rispoli, R. Schittko, P. M. Preiss, and M. Greiner, Science **353**, 794 (2016).
[8] J. Choi, H. Zhou, S. Choi, R. Landig, W. W. Ho, J. Isoya, F. Jelezko, S. Onoda, H. Sumiya, D. A. Abanin, and M. D. Lukin, Phys. Rev. Lett. **122**, 043603 (2019).
[9] Y. Tang, W. Kao, K.-Y. Li, S. Seo, K. Mallayya, M. Rigol, S. Gopalakrishnan, and B. L. Lev, Phys. Rev. X **8**, 021030 (2018).
[10] G. Clos, D. Porras, U. Warring, and T. Schaetz, Phys. Rev. Lett. **117**, 170401 (2016).
[11] H. Kim, Y. Park, K. Kim, H.-S. Sim, and J. Ahn, Phys. Rev. Lett. **120**, 180502 (2018).
[12] S. Lepoutre, J. Schachenmayer, L. Gabardos, B. Zhu, B. Naylor, E. Maréchal, O. Gorceix, A. M. Rey, L. Vernac, and B. Laburthe-Tolra, Nat. Commun. **10**, 1714 (2019).
[13] S. Hofferberth, I. Lesanovsky, B. Fischer, T. Schumm, and J. Schmiedmayer, Nature (London) **449**, 324 (2007).
[14] *Quantum Chaos: Between Order and Disorder*, edited by G. Casati and B.V. Chirikov, (Cambridge University Press, Cambridge, England, 1994).
[15] F. Haake, S. Gnutzmann, M. Kús, *Quantum signatures of chaos*, Springer Series in Synergetics (Springer, Cham, 2018).
[16] V. Zelevinsky, B. A. Brown, M. Horoi, and N. Frazier, Phys. Rep. **276**, 85 (1996).
[17] F. M. Izrailev, Phys. Rep. **196**, 299 (1990).
[18] T. A. Brody, J. Flores, J. B. French, P. A. Mello, A. Pandey, and S. S. M. Wong, Rev. Mod. Phys. **53**, 385 (1981).
[19] T. Guhr, A. Müller-Groeling, and H. A. Weidenmüller, Phys. Rep. **299**, 189 (1998).
[20] Y. Alhassid, Rev. Mod. Phys. **72**, 895 (2000).
[21] C. W. J. Beenakker, Rev. Mod. Phys. **69**, 731 (1997).
[22] J. M. Deutsch, Phys. Rev. A **43**, 2046 (1991).
[23] M. Srednicki, Phys. Rev. E **50**, 888 (1994).
[24] M. Rigol, V. Dunjko, and M. Olshanii, Nature **452**, 854 (2008).
[25] R. V. Jensen and R. Shankar, Phys. Rev. Lett. **54**, 1879 (1985).
[26] M. Feingold and A. Peres, Phys. Rev. A **34**, 591 (1986).
[27] M. Feingold, D. Leitner, and M. Wilkinson, Phys. Rev. Lett. **66**, 986 (1991).
[28] R. Steinigeweg, J. Herbrych, and P. Prelovšek, Phys. Rev. E **87**, 012118 (2013).
[29] W. Beugeling, R. Moessner, and M. Haque, Phys. Rev. E **89**, 042112 (2014).
[30] H. Kim, T. N. Ikeda, D. A. Huse, Phys. Rev. E **90**, 052105 (2014).
[31] E. J. Torres-Herrera and L. F. Santos, Phys. Rev. E **89**, 062110 (2014).
[32] R. Mondaini, K. R. Fratus, M. Srednicki, and M. Rigol, Phys. Rev. E **93**, 032104 (2016).
[33] R. Mondaini and M. Rigol, Phys. Rev. E **96**, 012157 (2017).
[34] D. Jansen, J. Stolpp, L. Vidmar, and F. Heidrich-Meisner, Phys. Rev. B **99**, 155130 (2019).
[35] T. LeBlond, K. Mallayya, L. Vidmar, and M. Rigol, Phys. Rev. E **100**, 062134 (2019).
[36] M. Brenes, T. LeBlond, J. Goold, and M. Rigol, Phys. Rev. Lett. **125**, 070605 (2020).
[37] J. Richter, A. Dymarsky, R. Steinigeweg, and J. Gemmer,

Phys. Rev. E **102**, 042127 (2020).
[38] J. D. Noh, Phys. Rev. E **103**, 012129 (2021).
[39] J. Richter, J. Gemmer, and R. Steinigeweg, Phys. Rev. E **99**, 050104(R) (2019).
[40] A. Dymarsky and K. Pavlenko, Phys. Rev. Lett. **123**, 111602 (2019).
[41] K. Kaneko, E. Iyoda, and T. Sagawa, Phys. Rev. A **101**, 042126 (2020).
[42] M. Mierzejewski and L. Vidmar, Phys. Rev. Lett. **124**, 040603 (2020).
[43] M. Brenes, S. Pappalardi, J. Goold, and A. Silva, Phys. Rev. Lett. **124**, 040605 (2020).
[44] M. Serbyn, D. A. Abanin, and Z. Papić, Nat. Phys. **17**, 675 (2021).
[45] G. Casati, L. Molinari, and F. Izrailev, Phys. Rev. Lett. **64**, 1851 (1990).
[46] Y. V. Fyodorov and A. D. Mirlin, Phys. Rev. Lett. **67**, 2405 (1991).
[47] V. K. B. Kota, Phys. Rep. **347**, 223 (2001).
[48] J. B. French and S. S. M. Wong, Phys. Lett. B **33**, 449 (1970).
[49] J. Flores, M. Horoi, M. Müller, and T. H. Seligman, Phys. Rev. E **63**, 026204 (2001).
[50] D. J. Luitz, I. M. Khaymovich, and Y. Bar Lev, SciPost Phys. Core **2**, 006 (2020).
[51] Y. Alhassid and R. D. Levine, Phys. Rev. Lett. **57**. 2879 (1986).
[52] Y. Alhassid and M. Feingold, Phys. Rev. A **39**, 374 (1989).
[53] C. I. Barbosa, T. Guhr, and H. L. Harney, Phys. Rev. E **62**, 1936 (2000).
[54] A. Dymarsky and H. Liu, Phys. Rev. E **99**, 010102 (2019).
[55] S. Hortikar, M. Srednicki, Phys. Rev. E **57**, 7313 (1998).
[56] S. Hortikar, M. Srednicki, Phys. Rev. E **61**, R2180(R) (2000).
[57] B. Eckhardt and J. Main, Phys. Rev. Lett. **75**, 2300 (1995).
[58] A. Dymarsky, arXiv:1804.08626.
[59] M. Brenes, S. Pappalardi, M. T. Mitchison, J. Goold, and A. Silva, Phys. Rev. E **104**, 034120 (2021).
[60] L. Foini and J. Kurchan, Phys. Rev. E **99**, 042139 (2019).
[61] A. Chan, A. De Luca, and J. T. Chalker, Phys. Rev. Lett. **122**, 220601 (2019).
[62] C. Murthy and M. Srednicki, Phys. Rev. Lett. **123**, 230606 (2019).
[63] B. Swingle, G. Bentsen, M. Schleier-Smith, and P. Hayden Phys. Rev. A **94**, 040302(R) (2016).
[64] J. Cotler, N. Hunter-Jones, J. Liu, and Beni Yoshida, J. High Energ. Phys. **2017**, 48 (2017).
[65] J. Cotler and N. Hunter-Jones, J. High Energ. Phys. **2020**, 205 (2020).
[66] S. Moudgalya, T. Devakul, C. W. von Keyserlingk, and S. L. Sondhi, Phys. Rev. B **99**, 094312 (2019).
[67] M. Schiulaz, E. J. Torres-Herrera, and L. F. Santos, Phys. Rev. B **99**, 174313 (2019).
[68] B. Bertini, F. Heidrich-Meisner, C. Karrasch, T. Prosen, R. Steinigeweg, and M. Žnidarič, Rev. Mod. Phys. **93**, 025003 (2021).
[69] D. A. Abanin, E. Altman, I. Bloch, and M. Serbyn, Rev. Mod. Phys. **91**, 021001 (2019).
[70] D. J. Thouless, Phys. Rep. **13**, 93 (1974).
[71] The thermalization time $\tau_{\rm th}$ can be intepreted as a generalization of the original "Thouless time" in the context of transport [70], as an excitation takes this time to diffuse across the system, cf. discussion around Eq. (8). The inverse scale $2\pi/\tau_{\rm th}$ marks the frequency below which $f(\bar{E},\omega)$ [Eq. (1)] is approximately constant, sometimes called Thouless energy [72]. At the same time, the notion of "Thouless energy" $\Delta E_{\rm TH}$ has also been associated with applicability of RMT to the energy spectrum [67, 73–76]. In some cases, $\Delta E_{\rm Th} \approx 2\pi/\tau_{\rm th}$.
[72] M. Serbyn, Z. Papić, and D. Abanin, Phys. Rev. B **96**, 104201 (2017).
[73] J. Šuntajs, J. Bonča, T. Prosen, L. Vidmar, Phys. Rev. E **102**, 062144 (2020).
[74] P. Kos, B. Bertini, and T. Prosen, Phys. Rev. Lett. **126**, 190601 (2021).
[75] S. Moudgalya, A. Prem, D. A. Huse, and A. Chan, Phys. Rev. Research **3**, 023176 (2021).
[76] P. Sierant, D. Delande, and J. Zakrzewski Phys. Rev. Lett. **124**, 186601 (2020).
[77] F. Jin, D. Willsch, M. Willsch, H. Lagemann, K. Michielsen, and H. De Raedt, J. Phys. Soc. Jpn. **90**, 012001 (2021).
[78] T. Heitmann, J. Richter, D. Schubert, and R. Steinigeweg, Z. Naturforsch. A **75**, 421 (2020).
[79] See supplemental material for details on the meaning of Λ^T including its analytical evaluation for uncorrelated matrix elements, as well as details on other random-matrix indicators beyond Λ^T, OTOCs, the accuracy of our typicality approach, additional numerical data on ETH indicators for $\mathcal{H}$, and for other models and observables, including Ref. [80].
[80] C. E. Porter and R. G. Thomas, Phys. Rev. **104**, 483 (1956).
[81] H. Tal-Ezer and R. Kosloff, J. Chem. Phys. **81**, 3967 (1984).
[82] V. V. Dobrovitski and H. De Raedt, Phys. Rev. E **67**, 056702 (2003).
[83] A. Weiße, G. Wellein, A. Alvermann, and H. Fehske, Rev. Mod. Phys. **78**, 275 (2006).
[84] C. Bartsch and J. Gemmer, Phys. Rev. Lett. **102**, 110403 (2009).
[85] In our simulations, we choose $M = 6aT$, which yields quite accurate values for Λ^T [79], but is still low enough such that numerical costs remain reasonable.
[86] Y. Yamaji, T. Suzuki, and M. Kawamura, arXiv:1802.02854.
[87] S. Garnerone and T. R. de Oliveira, Phys. Rev. B **87**, 214426 (2013).
[88] P. Sierant, D. Delande, and J. Zakrzewski Phys. Rev. Lett. **125**, 156601 (2020).
[89] R. Steinigeweg, A. Khodja, H. Niemeyer, C. Gogolin, and J. Gemmer, Phys. Rev. Lett. **112**, 130403 (2014).
[90] H. Kim and D. A. Huse, Phys. Rev. Lett. **111**, 127205 (2013).
[91] V. Oganesyan and D. A. Huse, Phys. Rev. B **75**, 155111 (2007).
[92] D. Cohen and T. Kottos, Phys. Rev. E **63**, 036203 (2001).
[93] T. Kottos and D. Cohen, Phys. Rev. E **64**, 065202(R) (2001).
[94] T. Elsayed and B. Fine, Phys. Rev. Lett. **110**, 070404 (2013).
[95] $C(t \to \infty)$ is numerically obtained as an average over fluctuations at long times. While the definition of $\tau_{\rm th}$ is not unique, our employed criterion remains numerically well controlled for all L.

[96] This leads to small and comparable statistical errors for all L considered here.
[97] T. L. M. Lezama, E. J. Torres-Herrera, F. Pérez-Bernal, Y. Bar Lev, and L. F. Santos, Phys. Rev. B **104**, 085117 (2021).
[98] S. Gopalakrishnan and S. A. Parameswaran, Phys. Rep. **862**, 1 (2020).

SUPPLEMENTAL MATERIAL

EVALUATION OF Λ^T FOR MATRICES WITH UNCORRELATED ELEMENTS

In the main text, we have introduced $\Lambda^T = \mathcal{M}_2^2/\mathcal{M}_4$ [Eq. (3)] as an indicator for the onset of "random-matrix behavior" ($\Lambda^T \to 0.5$), in the sense that the operator submatrix $\mathcal{O}^T$ within an energy window of width $2\pi/T$ is well described by a random matrix drawn for instance from a Gaussian Orthogonal Ensemble (GOE) and, in particular, that the matrix elements $\mathcal{O}^T_{mn}$ can be regarded as *uncorrelated* random numbers. Here, we provide more details on why Λ^T is indeed a useful quantity even if the matrix is not an instance of a GOE and how to nevertheless interpret the possible outcomes $\Lambda^T \neq 0.5$ or $\Lambda^T \to 0.5$.

To begin with, we note that for physical operators fulfilling the ETH [Eq. (1) in main text], the variances of off-diagonal matrix elements $|\mathcal{O}_{mn}|^2$ typically decay rapidly with energy distance ω as described by the envelope function $f(\bar{E},\omega)$, except for a narrow region around the diagonal where $f(\bar{E},\omega)$ is approximately constant. For small T, i.e., large energy windows, the submatrices $\mathcal{O}^T$ therefore probe a region where $f(\bar{E},\omega)$ is non-constant and therefore $\mathcal{O}^T_{mn}$ is trivially not described by a GOE, see also Fig. S3 below. Thus, one might expect that even if the r_{mn} in Eq. (1) are uncorrelated random numbers, the level density of $\mathcal{O}^T$ can differ from a semicircle and Λ^T can deviate from the GOE value $\Lambda^T_{\rm GOE} = 0.5$.

For small system sizes L, which are accessible by full exact diagonalization, we have demonstrated in Fig. 1 in the main text that it is insightful to compare $\mathcal{O}^T_{mn}$ with a sign-randomized version $\widetilde{\mathcal{O}}^T_{mn}$ [see Eq. (7) in main text]. In particular, while we find $\Lambda^T \neq 0.5$ for $\mathcal{O}^T$ and small T, the sign-randomized operator $\widetilde{\mathcal{O}}^T$ in contrast yields the GOE value $\Lambda^T = 0.5$, indicating that matrix elements $\mathcal{O}^T_{mn}$ exhibit correlations that are destroyed due to the sign-randomization. For larger L, for which we have to rely on the typicality approach, such a comparison is not possible anymore. Nevertheless, as we will show in the following, the emergence of $\Lambda^T = 0.5$ crucially does not depend on $f(\bar{E},\omega) = \text{const.}$, but can be derived solely by assuming that the r_{mn} are uncorrelated and by imposing some mild conditions on the matrix structure of $\mathcal{O}^T$.

To this end, let us write the fourth moment $\mathcal{M}_4$ in the energy basis,

$$\mathcal{M}_4 = \frac{1}{d}\sum_{mnkl} (\mathcal{O}^T_c)_{mn}(\mathcal{O}^T_c)_{nk}(\mathcal{O}^T_c)_{kl}(\mathcal{O}^T_c)_{lm} \ . \tag{S1}$$

Assuming that the elements $(\mathcal{O}^T_c)_{mn}$ are uncorrelated, only the "square" terms in the summation of Eq. (S1) are non-negligible. Thus, one gets (we omit the subscript c in $\mathcal{O}^T_c$ for simplicity in the following),

$$\begin{aligned}\mathcal{M}_4 &= \frac{1}{d}\sum_{mnl}|\mathcal{O}^T_{mn}|^2|\mathcal{O}^T_{lm}|^2 + \frac{1}{d}\sum_{mnk}|\mathcal{O}^T_{mn}|^2|\mathcal{O}^T_{kn}|^2 \\ &\quad - \frac{1}{d}\sum_{mn}|\mathcal{O}^T_{mn}|^4 \\ &= \frac{2}{d}\sum_m\Big(\sum_n|\mathcal{O}^T_{mn}|^2\Big)^2 - \frac{1}{d}\sum_{mn}|\mathcal{O}^T_{mn}|^4 \\ &= \frac{2}{d}\sum_m \mathcal{F}_m^2 - \frac{1}{d}\sum_{mn}|\mathcal{O}^T_{mn}|^4 \ ,\end{aligned}$$

where we have introduced,

$$\mathcal{F}_m = \sum_n |\mathcal{O}^T_{mn}|^2 = \langle m|(\mathcal{O}^T)^2|m\rangle \ , \tag{S2}$$

which will play a central role in the following. Let us further introduce the averages,

$$\langle\mathcal{F}\rangle = \frac{1}{d}\sum_m \mathcal{F}_m \ , \quad \langle\mathcal{F}^2\rangle = \frac{1}{d}\sum_m \mathcal{F}_m^2 \ , \tag{S3}$$

and the variance,

$$\sigma^2_{\mathcal{F}} = \frac{1}{d}\sum_m(\mathcal{F}_m - \langle\mathcal{F}\rangle)^2 \ . \tag{S4}$$

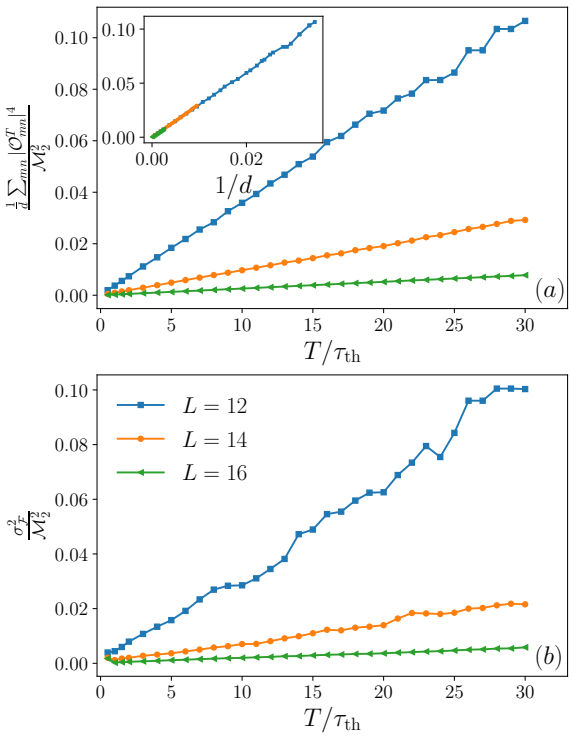


FIG. S1. (a) $\frac{1}{d}\sum_{mn}|\mathcal{O}^T_{mn}|^4/\mathcal{M}_2^2$ versus $T/\tau_{\rm th}$ and (b) $\sigma^2_{\mathcal{F}}/\mathcal{M}_2^2$ versus $T/\tau_{\rm th}$ for $\mathcal{A}$ with $q = \frac{L}{2}$, obtained for the Ising model of the main text and system sizes $L = 12, 14, 16$. Inset in (a) shows $\frac{1}{d}\sum_{mn}|\mathcal{O}^T_{mn}|^4/\mathcal{M}_2^2$ versus $1/d$.

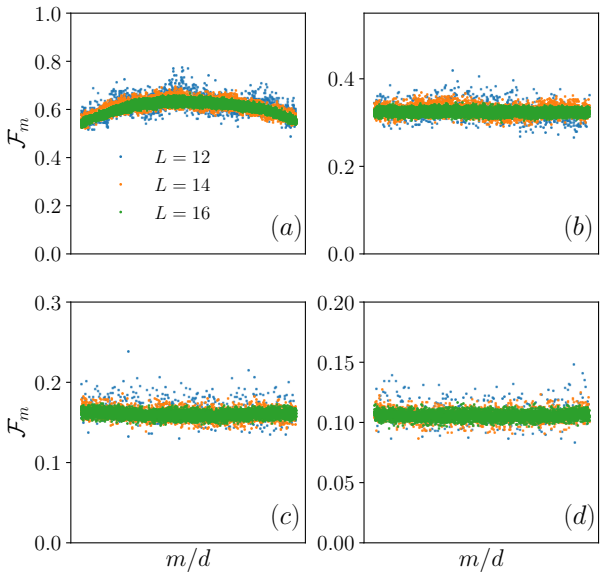


FIG. S2. $\mathcal{F}_m$ for the density-wave operator $\mathcal{A}(q = \frac{L}{2})$ in the Ising model of the main text with $L = 12, 14, 16$. Data is obtained in energy windows $\Delta E = 2\pi/T$ with (a) $T = 0.5\tau_{\rm th}$, (b) $T = 1\tau_{\rm th}$, (c) $T = 2\tau_{\rm th}$, (d) $T = 3\tau_{\rm th}$.

Then we can write,

$$\begin{aligned}\mathcal{M}_4 &= 2\langle\mathcal{F}^2\rangle - \frac{1}{d}\sum_{mn}|\mathcal{O}^T_{mn}|^4 \\ &= 2\langle\mathcal{F}\rangle^2 + 2\sigma^2_{\mathcal{F}} - \frac{1}{d}\sum_{mn}|\mathcal{O}^T_{mn}|^4 \\ &= 2\mathcal{M}_2^2 + 2\sigma^2_{\mathcal{F}} - \frac{1}{d}\sum_{mn}|\mathcal{O}^T_{mn}|^4 \ , \end{aligned} \tag{S5}$$

where we used $\langle\mathcal{F}\rangle^2 = \mathcal{M}_2^2$. Substituting Eq. (S5) into the definition of Λ^T yields

$$\begin{aligned}\Lambda^T = \frac{\mathcal{M}_2^2}{\mathcal{M}_4} &= \frac{\mathcal{M}_2^2}{2\mathcal{M}_2^2 + 2\sigma^2_{\mathcal{F}} - \frac{1}{d}\sum_{mn}|\mathcal{O}^T_{mn}|^4} \\ &\simeq 0.5 - \left(\frac{\sigma^2_{\mathcal{F}}}{2\mathcal{M}_2^2} - \frac{\frac{1}{d}\sum_{mn}|\mathcal{O}^T_{mn}|^4}{4\mathcal{M}_2^2}\right) \ . \end{aligned} \tag{S6}$$

So far, we only assumed that the $\mathcal{O}^T_{mn}$ are uncorrelated. In the following, we will demonstrate that the expressions in the bracket of Eq. (S6) will be negligibly small under reasonably mild requirements on the matrix structure of $\mathcal{O}^T$. First of all, as we consider central moments here, the variance of the diagonal and off-diagonal elements of $\mathcal{O}^T$ should be of the same order if T is sufficiently large and $\mathcal{O}^T$ satisfies ETH. (For the density wave operator that we mainly focus in the main text, this is always the case even if T is quite small.) As a consequence,

$$\frac{\frac{1}{d}\sum_{mn}|\mathcal{O}^T_{mn}|^4}{\mathcal{M}_2^2} \propto \frac{1}{d} \ , \tag{S7}$$

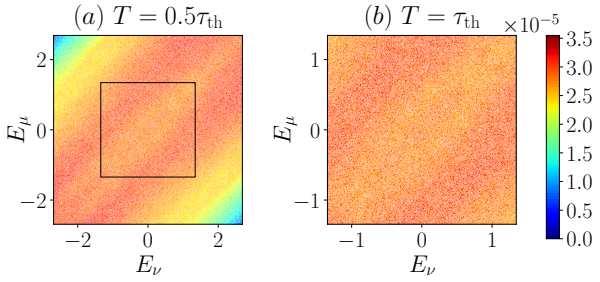


FIG. S3. Coarse grained matrix representation of $\mathcal{A}(q = L/2)$ in the eigenbasis of $\mathcal{H}$, i.e., averaged squared matrix elements in bins of width $\Delta_{\rm bin}$, $\frac{1}{\Delta^2_{\rm bin}}\sum_{m=\mu}^{\mu+\Delta_{\rm bin}}\sum_{n=\nu}^{\nu+\Delta_{\rm bin}}|\langle m|\mathcal{A}|n\rangle|^2$. Data is shown for $L = 16$ in two different energy windows $\Delta E = \frac{\pi}{T}$ with (a) $T = \tau_{\rm th}/2$ and (b) $T = \tau_{\rm th}$. The box in (a) indicates the energy window shown in (b). Note that this data can be interpreted as a visualization of the squared function $f^2(\bar{E}, \omega)$ in the ETH ansatz.

which can therefore be neglected in the case of large d. We demonstrate this fact numerically in Fig. S1 (a). In particular, we find that the left hand side of Eq. (S7) is indeed quite small for $L = 16$ and scales as $1/d$.

Secondly, we consider the quantity $\mathcal{F}_m$ introduced in Eq. (S2). In particular, if we assume that $\mathcal{O}^T$ obeys a certain stiffness in the sense that $\mathcal{F}_m$ does not depend strongly on m, the variance $\sigma^2_{\mathcal{F}}$ will be small such that,

$$\frac{\sigma^2_{\mathcal{F}}}{\mathcal{M}_2^2} \ll 1 \ . \tag{S8}$$

As demonstrated in Fig. S1 (b), we find that this condition is indeed well fulfilled for the models and operators considered here and that $\sigma^2_{\mathcal{F}}/\mathcal{M}_2^2$ quickly decreases with increasing system size. Moreover, in Fig. S2, we plot $\mathcal{F}_m$ for exemplary energy windows $\Delta E = \frac{2\pi}{T}$, emphasizing that fluctuations decrease with increasing L and are already quite small even in energy windows corresponding to $T = \tau_{\rm th}$.

Combining Eqs. (S6), (S7), and (S8), one thus finds,

$$\Lambda^T \simeq 0.5 \ , \tag{S9}$$

which is just the prediction of the Wigner semicircle spectrum. Let us stress that deriving Eq. (S9) only required that matrix elements are uncorrelated and, as a main assumption, that the fluctuations of $\mathcal{F}_m$ are small. In particular $\mathcal{O}^T_{mn}$ not necessarily have to follow a strict GOE in the sense that $f(\bar{E}, \omega)$ can vary within the chosen energy window. This also explains why the sign-randomized operator yields the random-matrix value $\Lambda^T = 0.5$ even for small T (see Fig. 1 in main text), where $f(\bar{E}, \omega)$ is non-constant (see Fig. S3). While we cannot prove that $\sigma_{\mathcal{F}}$ will stay small also for system sizes beyond the ones studied in Figs. S1 and S2, we think that this is a reasonable assumption. Thus, $\Lambda^T \to 0.5$ remains a meaningful indi-

cator for the emergence of uncorrelated matrix elements, the exploration of which is a main goal of this work.

LEVEL-SPACING STATISTICS OF OPERATOR SUBMATRICES

Let us present additional data supporting that Λ^T is indeed a very useful and sensitive indicator for the presence of correlations between matrix elements. To this end, let us study another very common "random-matrix indicator", i.e., the mean ratio $\langle r_T\rangle$ of the adjacent level spacings [S1],

$$\langle r_T\rangle = \frac{1}{d}\sum_\alpha \frac{\min(\Delta_\alpha,\Delta_{\alpha+1})}{\max(\Delta_\alpha,\Delta_{\alpha+1})}, \tag{S10}$$

where $\Delta_\alpha = |\lambda^T_{\alpha+1} - \lambda^T_\alpha|$ denotes the gap between two adjacent eigenvalues λ^T_α of $\mathcal{O}^T$, and the averaging is performed over all the gaps in the energy window. For a random matrix drawn from the GOE, $r_{\rm GOE}\approx 0.53$, while for the uncorrelated Poisson distributed eigenvalues, one finds $r_{\rm Poisson}\approx 0.39$. As can be seen from Fig. S4, for both operators $\mathcal{A}(q=L/2)$ and $\mathcal{A}(q=1)$, we find that $\langle r_T\rangle$ is close to the GOE value for the entire range of T shown here. In this context, let us stress that our comparison with the sign-randomized operator in Fig. 1 in the main text has unveiled that the matrix elements of $\mathcal{O}^T$ clearly exhibit correlations at small T, manifest in a value $\Lambda^T\neq 0.5$. In contrast, as demonstrated in Fig. S4, $\langle r_T\rangle$ is not sensitive to this transition from correlated to uncorrelated matrix elements with increasing T.

REDUCTION OF OTOC TO TWO-POINT CORRELATION FUNCTIONS

Let us provide details on the relation $F_T(t)\approx 2\overline{C}_T(t)$ valid in case matrix elements of $\mathcal{O}^T_c$ are uncorrelated, which we used in the context of Fig. 4 in the main text. In the energy eigenbasis, the out-of-time-ordered correlator $F_T(t)$ can be written as,

$$F_T(t) = \sum_{mnkl} \mathcal{O}^T_{mn}\mathcal{O}^T_{nk}\mathcal{O}^T_{kl}\mathcal{O}^T_{lm} e^{-i(E_n-E_m+E_l-E_k)t}. \tag{S11}$$

Assuming that matrix elements $\mathcal{O}^T_{mn}$ are uncorrelated, as well as the variances of the diagonal and off-diagonal elements of $\mathcal{O}^T_c$ are of same order, one finds (see also [S2]),

$$\begin{aligned} F_T(t) &\simeq \sum_m\sum_n |\mathcal{O}^T_{mn}|^2 e^{-i(E_n-E_m)t}\sum_l |\mathcal{O}^T_{ml}|^2 e^{-i(E_l-E_m)t} \\ &+ \sum_n\sum_m |\mathcal{O}^T_{nm}|^2 e^{-i(E_n-E_m)t}\sum_l |\mathcal{O}^T_{nk}|^2 e^{-i(E_n-E_k)t} \\ &= \sum_m (\sum_n |\mathcal{O}^T_{mn}|^2 e^{-i(E_n-E_m)t})^2 + c.c. \\ &= 2\sum_m \Re\left((\langle m|\mathcal{O}^T(t)\mathcal{O}^T|m\rangle)^2\right) \\ &= 2\overline{C}_T(t)\ . \end{aligned} \tag{S12}$$

where we used arguments similar to Eq. (S1) above.

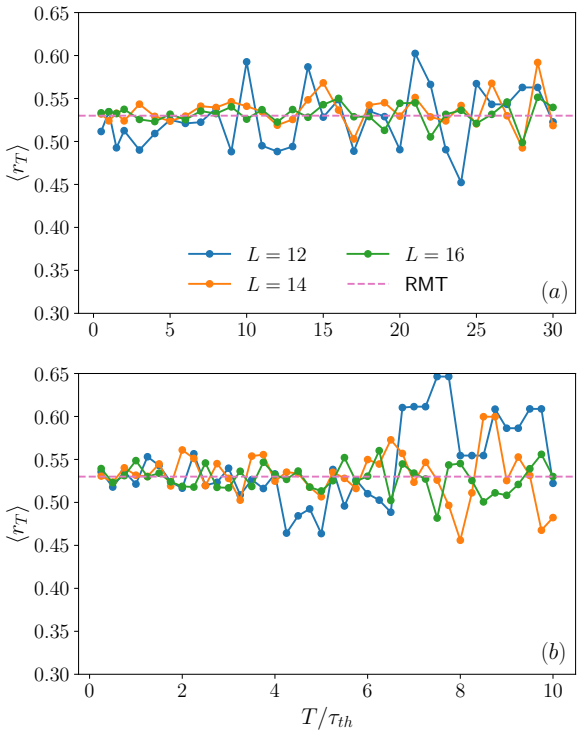


FIG. S4. Mean adjacent gap ratio $\langle r_T\rangle$ for the density wave operator $\mathcal{A}$ with (a) $q = L/2$ and (b) $q = 1$, obtained within different energy window $\Delta E = 2\pi/T$ and system sizes $L = 12, 14, 16$ for the Ising model $\mathcal{H}$ of the main text.

DETAILS ON THE NUMERICAL APPROACH

In this section, we provide more details on our numerical approach, based on quantum typicality, which is used to simulate the random-matrix indicator Λ^T and the dynamical correlation function $C(t)$.

Implementing the energy filter and calculating Λ^T

To begin with, it is useful to rewrite $\exp[-i(\mathcal{H}-E_0)t]$ as

$$\exp(-i(\mathcal{H}-E_0)t) = \exp(-i(b-E_0)t)\exp(-iat\frac{\mathcal{H}-b}{a}), \tag{S13}$$

where the second term can be expanded in terms of Chebyshev polynomials of the first kind [denoted by $T_k(x)$],

$$\exp(-iat\frac{\mathcal{H}-b}{a}) = J_0(at)+2\sum_{k=1}^{\infty}(-i)^k J_k(at)T_k(\frac{\mathcal{H}-b}{a}) , \tag{S14}$$

where $a=(E_{\max}-E_{\min})/2$, $b=(E_{\max}+E_{\min})/2$, and J_k are Bessel functions of the first kind and order k. Substituting Eqs. (S13) and (S14) into the definition of P_T in the main text, one has

$$\begin{aligned} P_T &= \frac{1}{T}\int_{-\infty}^{+\infty}\mathrm{sinc}(\frac{t}{T})\exp(-i(\mathcal{H}-E_0)t)dt \qquad (S15)\\ &= \frac{1}{T}\int_{-\infty}^{+\infty}\mathrm{sinc}(\frac{t}{T})\exp(-i(b-E_0)t) \\ &\cdot\left[J_0(at)T_0(\frac{\mathcal{H}-b}{a})+2\sum_{k=1}^{\infty}(-i)^k J_k(at)T_k(\frac{\mathcal{H}-b}{a})\right]dt . \qquad (S16)\end{aligned}$$

After calculating the integral in Eq. (S16) analytically , one gets

$$P_T = \sum_{k=0}^{\infty} C_k T_k(\frac{\mathcal{H}-b}{a}) , \tag{S17}$$

where

$$C_0 = \frac{1}{\pi}\left(\frac{\arcsin(\frac{\pi}{T}+b-E_0)}{a} - \frac{\arcsin(-\frac{\pi}{T}+b-E_0)}{a}\right) , \tag{S18}$$

and

$$\begin{aligned} C_k(k\geq 1) = \frac{2(-1)^{k+1}}{\pi k}\Bigg[&\sin\left(k\arccos\left(\frac{\frac{\pi}{T}+b-E_0}{a}\right)\right) \\ &-\sin\left(k\arccos\left(\frac{-\frac{\pi}{T}+b-E_0}{a}\right)\right)\Bigg] , \end{aligned} \tag{S19}$$

under the condition

$$-a+b+\frac{\pi}{T} \leq E_0 \leq a+b-\frac{\pi}{T} , \tag{S20}$$

which is always fulfilled in our simulations as we only consider the middle region of the spectrum.

In order to study Eq. (S17) numerically, we consider only a finite number of terms in the summation,

$$P_T = \sum_{k=0}^{M} C_k T_k(\frac{\mathcal{H}-b}{a}) . \tag{S21}$$

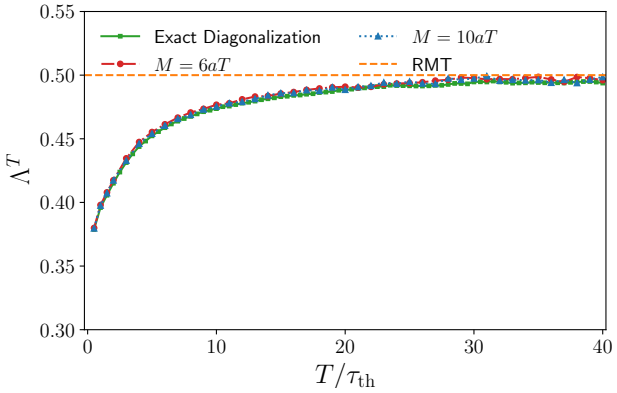


FIG. S5. Λ^T versus $T/\tau_{\rm th}$ for $\mathcal{A}(q=L/2)$ and system size $L=16$ in Ising model. Results are obtained by the typicality approach, averaged over 500 states, for two different value of $M=6aT$ (red) and $M=10aT$ (blue).

In our numerical simulations, we choose $M=6aT$, which yields quite accurate values for Λ^T, but is still low enough such that numerical costs remain reasonable. This is demonstrated in Fig. S5, where we compare the results of two different choices of M, $M=6aT$ and $M=10aT$. We find that the results are very similar and agree convincingly with the data obtained by exact diagonalization.

In our numerical approach, we calculate the moments $\mathcal{M}_k$ by making use of quantum typicality [S3, S4], where the energy filter P_T is applied to a random pure quantum state. The variance of the statistical error within this approach scales as $1/d$, where d is the effective dimension of the Hilbert space, i.e., the number of eigenstates within the energy window. For a fixed ΔE, our approximation becomes more accurate for larger system size L, as d usually scales exponentially with L. Even for moderate system sizes, one can improve the accuracy by averaging over N different realizations of random states, which can reduce the variance by a factor N. In our numerical simulations, N is adjusted as a function of system L, $N \propto \frac{1}{2^L}$, yielding accurate results for all system sizes considered by us.

Details on the typicality approach for the autocorrelation function

Given the operator $\mathcal{O}$, the its infinite-temperature autocorrelation function can be studied with quantum typicality as,

$$C(t) = \mathrm{Tr}[\mathcal{O}(t)\mathcal{O}]/2^L \simeq \langle\psi|\mathcal{O}(t)\mathcal{O}|\psi\rangle , \tag{S22}$$

where $|\psi\rangle$ is a pure state drawn at random from the unitarily invariant Haar measure, and $\langle\psi|\psi\rangle=1$. Introducing an auxiliary state $|\psi_{\mathcal{O}}\rangle = \mathcal{O}|\psi\rangle$, Eq. (S22) can be written as,

$$C(t) \simeq \langle\psi(t)|\mathcal{O}|\psi_{\mathcal{O}}(t)\rangle, \tag{S23}$$

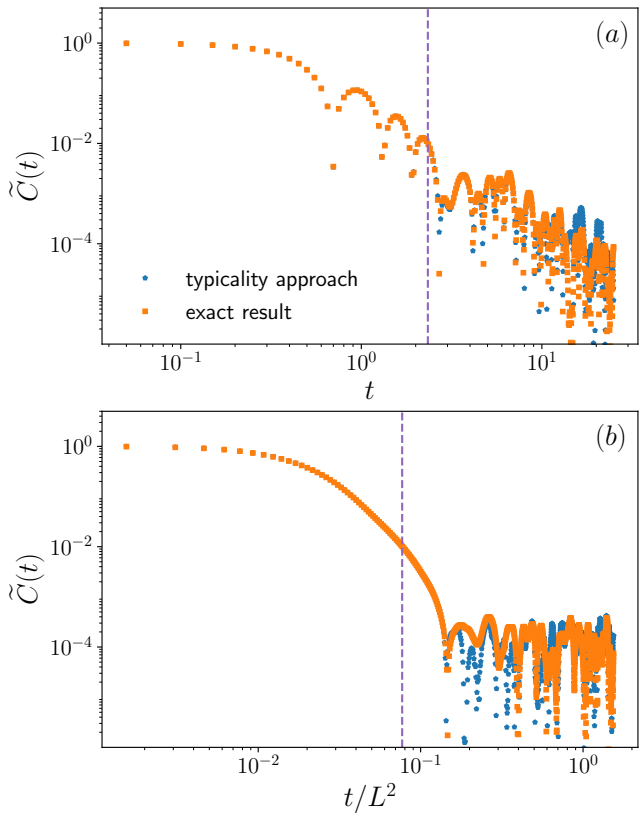


FIG. S6. Exact results of rescaled autocorrelation function $\widetilde{C}(t)$ versus data obtained by quantum typicality (averaged over 1000 random states) for (a) $\mathcal{A}(q=1)$ and (b) $\mathcal{A}(q=L/2)$ in the Ising model $\mathcal{H}$ with $L=16$. The dashed line signals the thermalization time $\tau_{\rm th}$ according to our definition in the main text.

where

$$|\psi(t)\rangle = \exp(-i\mathcal{H}t)|\psi\rangle, \quad |\psi_{\mathcal{O}}(t)\rangle = \exp(-i\mathcal{H}t)|\psi_{\mathcal{O}}\rangle \ , \tag{S24}$$

which can be efficiently simulated by means of sparse-matrix techniques.

It is well established that the error of the typicality approximation (S23) decreases exponentially for increasing system size [S4]. While this error becomes negligibly small for the larger values of L considered by us, it can again be reduced for smaller L by averaging over different realizations of random states. We demonstrate the accuracy of quantum typicality in Fig. S6, where we compare the dynamics obtained by quantum typicality (averaged over 1000 random states) with exact diagonalization data for the Ising model $\mathcal{H}$ with $L=16$. For both operators $\mathcal{A}(q=1)$ and $\mathcal{A}(q=L/2)$ considered here, we find that the typicality approach is very accurate, even at long times around $\tau_{\rm th}$, where $C(t)$ has decayed for rather small values.

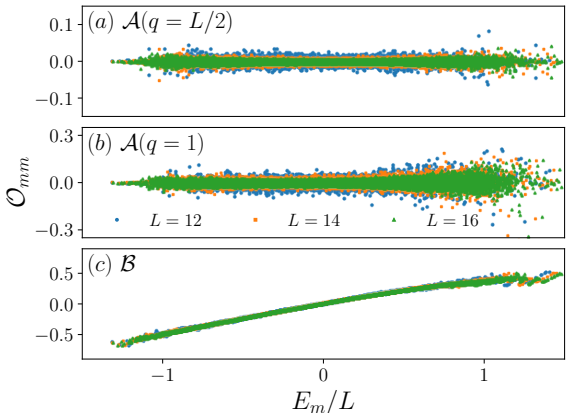


FIG. S7. Diagonal matrix elements of operators (a) $\mathcal{A}(q=L/2)$, (b) $\mathcal{A}(q=1)$, and (c) $\mathcal{B}$, in the eigenbasis of the Ising model $\mathcal{H}$ with $L=12,14,16$.

USUAL INDICATORS OF THE ETH AND QUANTUM CHAOS

Let us demonstrate that the operators considered in the main text are in good agreement with standard indicators of the ETH.

Diagonal matrix elements

As a first step, we study the diagonal part of the ETH. To this end, Fig. S7 shows the matrix elements $\langle m|\mathcal{A}|m\rangle$ and $\langle m|\mathcal{B}|m\rangle$, for different system sizes $L=12,14,16$ in the Ising model. For energy densities in the center of the spectrum, we find that the "cloud" of matrix elements becomes narrower with increasing L, which is in good accord with the ETH prediction that the $\mathcal{O}_{mm}$ should form a "smooth" function of energy in the thermodynamic limit $L\to\infty$, and that the fluctuation of $\mathcal{O}_{mm}$ decay exponentially with L.

Off-diagonal matrix elements

We now turn to the properties of the off-diagonal matrix elements $\mathcal{O}_{mn}$, where we focus on the eigenstates with mean energy $\bar{E}\in[-0.5,0.5]$. Assuming the $\mathcal{O}_{mn}$ have zero mean, i.e. $\overline{\mathcal{O}_{mn}}=0$, (which we find to hold to a very high accuracy), we study the frequency-dependent ratio $\Gamma(\omega)$, recently introduced in Ref. [S6],

$$\Gamma(\omega) = \frac{\overline{|\mathcal{O}_{mn}|^2}(\omega)}{[\overline{|\mathcal{O}_{mn}|}(\omega)]^2} \ , \tag{S25}$$

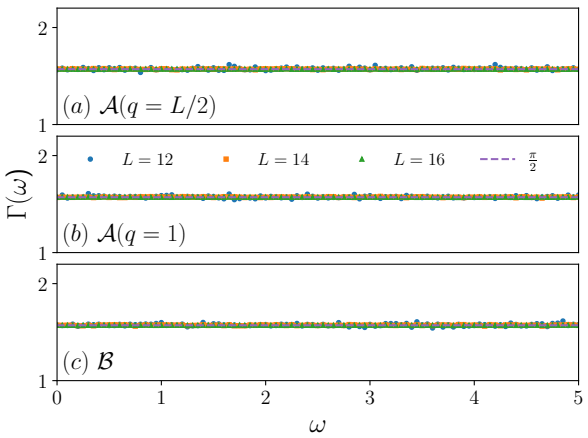


FIG. S8. $\Gamma(\omega)$ for matrix elements of operator (a) $\mathcal{A}(q = L/2)$, (b) $\mathcal{A}(q = 1)$, (c) $\mathcal{B}$, in the energy window $E \in [-0.5, 0.5]$ and system sizes $L = 12, 14, 16$ in Ising model.

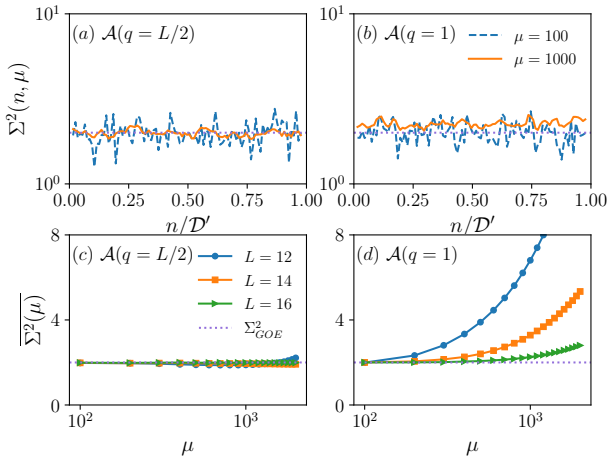


FIG. S9. [(a),(b)] Ratio $\Sigma^2(n, \mu)$ between the variances of diagonal and off-diagonal matrix elements for two different square sizes $\mu = 100, 1000$ and all embeddings $n \in [1 + \mu/2, \mathcal{D}' - \mu/2]$ for operator $\mathcal{A}$ in Ising model. The data are obtained for system size $L = 16$ and the dashed line indicates the RMT prediction $\Sigma^2_{\rm GOE} = 2$. [(c),(d)] Average value $\overline{\Sigma^2(\mu)}$ versus μ for system sizes $L = 12, 14, 16$. Panels (a) and (c) show data for $q = L/2$, while (b) and (d) show data for $q = 1$.

where,

$$\overline{|\mathcal{O}_{mn}|^2}(\omega) = \frac{1}{N_\omega} \sum_{\substack{m,n \\ |E_m - E_n| \approx \omega}} |\mathcal{O}_{mn}|^2 \,, \tag{S26}$$

$$\overline{|\mathcal{O}_{mn}|}(\omega) = \frac{1}{N_\omega} \sum_{\substack{m,n \\ |E_m - E_n| \approx \omega}} |\mathcal{O}_{mn}| \,. \tag{S27}$$

Here the sum runs over all N_ω matrix elements with $|E_m - E_n| \in |\omega - \Delta\omega/2, \omega + \Delta\omega/2|$, where we choose $\Delta\omega = 0.05$ in our numerical simulation. In Fig. S8 we find that $\Gamma(\omega)$ is close to the Gaussian value $\pi/2$ for almost all values of ω and L considered here, indicating a Gaussian distribution of $\mathcal{O}_{mn}$.

Furthermore, we also calculate the ratio $\Sigma^2(n, \mu)$ [S7–S9] between the variances of diagonal and off-diagonal matrix elements for eigenstates in regions $[n - \mu/2, n + \mu/2]$ of width μ (see also [S5]),

$$\Sigma^2(n, \mu) = \frac{\sigma^2_{\rm d}(n, \mu)}{\sigma^2_{\rm od}(n, \mu)} \,. \tag{S28}$$

In Figs. S9 (a) and S9 (b), we study the ratio $\Sigma^2(n, \mu)$ of the density-wave operator $\mathcal{A}$ for $q = L/2$ and $q = 1$, respectively. Specifically, the data are obtained for $L = 16$ with two different square sizes $\mu = 100, 1000$ and all possible embedding along the diagonal of the submatrix with dimension $\mathcal{D}' \approx \mathcal{D}/2$, where $\mathcal{D} = 2^L$ is the total dimension of the Hilbert space. We observe that $\Sigma^2(n, \mu)$ fluctuates around the GOE prediction $\Sigma^2_{\rm GOE} = 2$.

In Figs. S9 (c) and S9 (d), we show the averaged value

$$\overline{\Sigma^2(\mu)} = \frac{1}{\mathcal{D}' - \mu} \sum_{n=1+\mu/2}^{\mathcal{D}'-\mu/2} \Sigma^2(n, \mu) \,. \tag{S29}$$

We find that $\overline{\Sigma^2(\mu)} \approx \Sigma^2_{\rm GOE}$ for small μ, while it grows monotonously with increasing μ [this growth is particularly pronounced in the case of slowest mode $q = 1$ as shown in Fig. S9 (d)]. Comparing the results for different L, we find that $\overline{\Sigma^2(\mu)}$ remains closer to $\Sigma^2_{\rm GOE}$ for larger L, and it is reasonable to expect that $\overline{\Sigma^2(\mu)} \approx \Sigma^2_{\rm GOE}$ holds in the thermodynamic limit $L \to \infty$, indicating $\mathcal{O}_{mn}$ follow a Gaussian distribution, at least for m, n in the middle of the energy spectrum.

Eventually, we also study the distribution of the transition strengths, taking $\mathcal{A}$ with $q = L/2$ and $q = 1$ as probe operators. More specifically, we consider $y = \mathcal{A}^2_{mn}$, which should follow the Porter-Thomas distribution [S10], if the matrix elements are drawn according to a GOE. In Fig. S10, we take into account the matrix elements $\mathcal{A}^2_{mn}$ within the energy window $E_m, E_n \in [-\pi/\tau_{\rm th}, \pi/\tau_{\rm th}]$, and study the distribution of the rescaled transition strength $\widetilde{y} = \mathcal{A}^2_{mn}/\langle \mathcal{A}^2_{mn} \rangle$ [denoted by $f(\widetilde{y})$]. One can see that $f(\widetilde{y})$ can be well described by the Porter Thomas distribution (which is also the χ^2 distribution with one degree of freedom)

$$f_{\rm PT}(\widetilde{y}) = (2\pi)^{-1/2} \widetilde{y}^{-1/2} \exp(-\widetilde{y}/2), \tag{S30}$$

for both operators and all system sizes considered here.

NUMERICAL RESULTS OF Λ^T IN XXZ MODEL

In addition to the Ising model studied in the main text, we also consider a nonintegrable XXZ model with next-

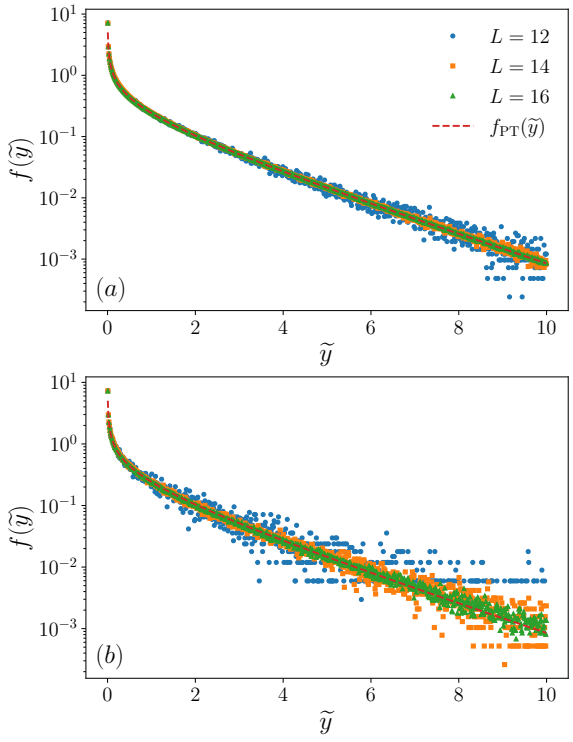


FIG. S10. Distribution of rescaled transition strength $\widetilde{y}$ for (a) $\mathcal{A}(q = L/2)$ and (b) $\mathcal{A}(q = 1)$ within the energy window $[-\pi/\tau_{\rm th}, \pi/\tau_{\rm th}]$. Data is obtained for the Ising model $\mathcal{H}$ with $L = 12, 14, 16$. The dashed line indicates the Porter-Thomas distribution, which is predicted by GOE.

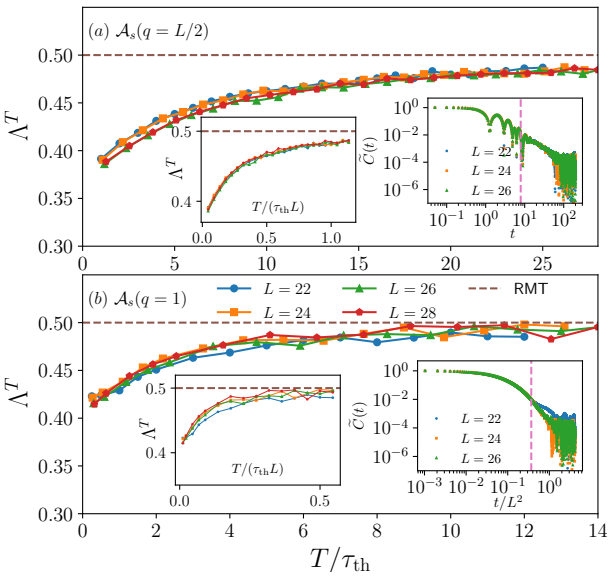


FIG. S11. Λ^T versus $T/\tau_{\rm th}$ for the spin density-wave operator $\mathcal{A}_s$ (S32) in XXZ model (described by $\mathcal{H}_2$) with (a) $q = L/2$ and (b) $q = 1$. Data is obtained using typicality approach, averaged over $500 \cdot 2^{L-18}$ states, for up to $L = 28$. The dashed horizontal line indicates the GOE value $\Lambda^T = 0.5$. The two insets show Λ^T versus $T/(\tau_{\rm th}L)$ and the rescaled autocorrelation function $\widetilde{C}(t)$ in log-log scale, obtained by typicality approach. The dashed vertical line signals the thermalization time $\tau_{\rm th}$ according to our definition. Good quality of collapse of $C(t)$ and $C(t/L^2)$ correspondingly for different L confirms L-independence of $\tau_{\rm th}$ for $q = L/2$ and diffusive behavior $\tau_{\rm th} \propto L^2$ for $q = 1$.

nearest neighbor interactions,

$$\mathcal{H}_2 = \sum_{\ell=1}^{L} s_x^\ell s_x^{\ell+1} + s_y^\ell s_y^{\ell+1} + \Delta_1 s_z^\ell s_z^{\ell+1} + \sum_{\ell=1}^{L} \Delta_2 s_z^\ell s_z^{\ell+2} + h_1 s_z^1 + h_{\lfloor \frac{L}{3} \rfloor + 1} s_z^{\lfloor \frac{L}{3} \rfloor + 1} , \quad \text{(S31)}$$

where $s^\ell_{x,y,z} = \frac{1}{2}\sigma^\ell_{x,y,z}$ are spin operators at lattice site ℓ, L is the length of the chain with periodic boundaries, and we choose $\Delta_1 = 1.5, \Delta_2 = 0.5, h_1 = 0.1, h_{\lfloor \frac{L}{3} \rfloor + 1} = 0.075$ ($\lfloor\rfloor$ indicates the floor function). The two defects are added to lift the translation and reflection symmetries. The zero magnetization subspace is considered and the energy center is chosen to be $E_0 = -0.3L/16$, corresponding to infinite temperature. We consider a spin density-wave operator,

$$\mathcal{A}_s = \sum_{\ell=1}^{L} \cos(\frac{2\pi}{L}\ell q) s_z^\ell , \quad \text{(S32)}$$

which exhibits slow hydrodynamics relaxation in the limit of small q.

In Fig. S11, analogous to the results obtained for the the Ising model in the main text, we find that $\Lambda^T \neq 0.5$ at small T, indicating the presence of correlations between matrix elements. Only at much longer times $T \gg \tau_{\rm th}$, we observe that $\Lambda^T \to 0.5$ suggesting a transition to genuine GOE behavior. Furthermore, by plotting Λ^T as a function of $T/(\tau_{\rm th}L)$, the good numerical collapse extending through almost all values of T tentatively suggests $T_{\rm RMT} \propto \tau_{\rm th}L$ for $\mathcal{A}_s$ with $q = L/2$, see inset in Fig. S11 (a). Note, however, that such a data collapse is less clear for $q = 1$, see inset in Fig. S11 (b).

Finally, in order to connect to the results presented in Ref. [S5], we also consider the next-nearest neighbor XXZ chain with the parameters used in [S5],

$$\mathcal{H}_3 = \sum_{\ell=1}^{L} s_x^\ell s_x^{\ell+1} + s_y^\ell s_y^{\ell+1} + \Delta_1 s_z^\ell s_z^{\ell+1} + \sum_{\ell=1}^{L} \Delta_2 s_z^\ell s_z^{\ell+2} + h_1 s_z^1, \quad \text{(S33)}$$

namely $h_1 = 0.1, \Delta_1 = 1.5, \Delta_2 = 1.2$, and open boundary conditions. As before, we consider the zero magnetization subspace. Moreover, we study a local operator $s_z^{\lfloor \frac{L}{2} \rfloor}$ in the middle of the chain, which exhibits a power-law relaxation (approximately $\propto t^{-1/2}$), see inset in Fig. S12. As shown in in Fig. S12, we find that although a

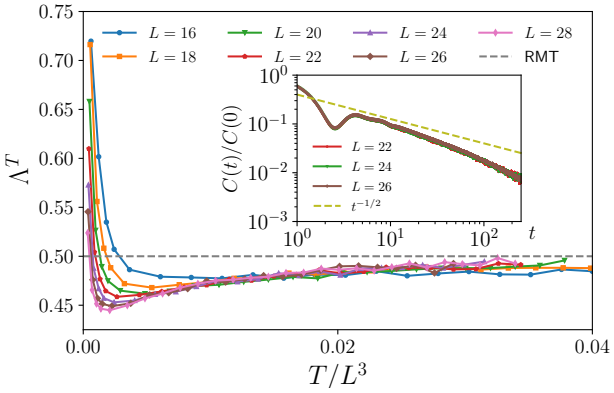


FIG. S12. Λ^T versus $T/\tau_{\rm th}$ for local operator $s_z^{\lfloor \frac{L}{2} \rfloor}$ in XXZ model $\mathcal{H}_3$. Data for $L = 16$ is obtained by exact diagonalization, while data for $L \geq 18$ is obtained by our typicality approach, averaged over $500 \cdot 2^{L-18}$ states. The dashed horizontal line indicates the RMT value $\Lambda^T = 0.5$. The inset shows the autocorrelation function $C(t)$, normalized by its initial value, where the dashed line indicates a $t^{-1/2}$ decay.

"sharp transition" to RMT seems to exist for small system sizes ($L = 16$), the analysis of longer chains unveils that $\Lambda^T \to 0.5$ only at times much longer than the thermalization time. Interestingly, we observe a good numerical collapse of all the curves as a function of T/L^3 (note that $t_{\rm th} \propto L^2$ for this operators), which is consistent with the analytical prediction in Ref. [S11].

* jiaozi.wang@uos.de
† jgemmer@uos.de

[S1] V. Oganesyan and D. A. Huse, Phys. Rev. B **75**, 155111 (2007).
[S2] M. Brenes, S. Pappalardi, M. T. Mitchison, J. Goold, and A. Silva, Phys. Rev. E **104**, 034120 (2021).
[S3] F. Jin, D. Willsch, M. Willsch, H. Lagemann, K. Michielsen, and H. De Raedt, J. Phys. Soc. Jpn. **90**, 012001 (2021).
[S4] T. Heitmann, J. Richter, D. Schubert, and R. Steinigeweg, Z. Naturforsch. A **75**, 421 (2020).
[S5] J. Richter, A. Dymarsky, R. Steinigeweg, and J. Gemmer, Phys. Rev. E **102**, 042127 (2020).
[S6] T. LeBlond, K. Mallayya, L. Vidmar, and M. Rigol, Phys. Rev. E **100**, 062134 (2019).
[S7] L. D'Alessio, Y. Kafri, A. Polkovnikov, and M. Rigol, Adv. Phys. **65**, 239 (2016).
[S8] R. Mondaini and M. Rigol, Phys. Rev. E **96**, 012157 (2017).
[S9] D. Jansen, J. Stolpp, L. Vidmar, and F. Heidrich-Meisner, Phys. Rev. B **99**, 155130 (2019).
[S10] C. E. Porter and R. G. Thomas, Phys. Rev. **104**, 483 (1956).
[S11] A. Dymarsky, arXiv:1804.08626.